The Journal of Neuroscience, May 1993, 13(5): 2001–2012

Differential Localization of Phosphoinositide-linked Metabotropic Glutamate Receptor (mGluR1) and the Inositol 1,4,5-Trisphosphate Receptor in Rat Brain

Majid Fotuhi,[1] Alan H. Sharp,[1] Charles E. Glatt,[1] Paul M. Hwang,[1] Marcus von Krosigk,[2] Solomon H. Snyder,[1] and Ted M. Dawson[1]

[1]Departments of Neuroscience, Neurology Pharmacology and Molecular Sciences, and Psychiatry, The Johns Hopkins University School of Medicine, Baltimore, Maryland 21205 and [2]Section of Neurobiology, Yale University Medical School, New Haven, Connecticut 06511

The type 1 metabotropic glutamate receptor (mGluR1) is thought to act via the phosphoinositide (PI) system with the associated formation of inositol 1,4,5-trisphosphate (IP_3) and Ca^{2+} release. Utilizing immunohistochemistry and *in situ* hybridization, we have localized protein and mRNA, respectively, for the mGluR1 and the IP_3 receptor (IP_3R). We have also localized glutamate-linked PI turnover by autoradiography with ^{3}H-cytidine. We observe a striking contrast in localizations of mGluR1 and IP_3R both for protein and mRNA. For instance, mGluR1 occurs in the apparent absence of IP_3R in neurons of the stratum oriens of the CA1 hippocampus, islands of Calleja, anterodorsal nucleus of thalamus, lateral nucleus of hypothalamus, and the granular cell layer and the deep nuclei of cerebellum. mGluR1 actions in these brain regions may primarily be mediated through the protein kinase C limb of the PI system, as they contain moderate amounts of ^{3}H-phorbol ester binding. The subthalamic nucleus, red nucleus, and Darkshevich's nucleus, which possess high levels of mGluR1, are devoid of both IP_3R immunoreactivity and ^{3}H-phorbol ester binding. These reciprocal localizations suggest that mGluR1 actions in many brain areas may not primarily involve IP_3, reflecting instead influences on protein kinase C or other second messengers.

[Key words: excitatory amino acid receptors, protein kinase C, phospholipase C, in situ hybridization, immunohistochemistry]

Glutamate, the major excitatory neurotransmitter in the brain, acts through two major classes of receptors (Mayer and Westbrook, 1987; Collingridge and Lester, 1989; Monaghan et al., 1989; Miller, 1991a,b). At ionotropic receptors, glutamate directly opens ion channels. More recently, glutamate has been shown to act through a metabotropic glutamate receptor (mGluR) whereby phosphoinositide (PI) turnover is enhanced (for review, see Schoepp et al., 1990, Miller, 1991a; Baskys, 1992) via a G-protein mechanism (Nicoletti et al., 1988). Localizing neurotransmitter receptors provides valuable clues to their function. The ionotropic glutamate receptors have been localized by autoradiography with various ligands (for review, see Monaghan et al., 1989; Young and Fagg, 1990). Such localization has not been feasible for mGluR because of the lack of suitable ligands. Recently, we developed a technique to visualize PI turnover in brain slices utilizing ^{3}H-cytidine as a precursor to the PI cycle and could demonstrate selective enhancement in discrete brain structures by glutamate derivatives (Hwang et al., 1990a). However, the limited resolution of this technique has precluded detailed analysis of mGluR localizations. mGluR has been molecularly cloned (Houamed et al., 1991; Masu et al., 1991) and four subtypes identified (Tanabe et al., 1992). mGluR1 is PI linked, and alternative splicing yields a long and short form designated mGluR1α and mGluR1β, respectively. In addition, mGluR1 receptor stimulation leads to increased cAMP formation and release of arachidonic acid (Aramori and Nakinishi, 1992), mGluR2 activation inhibits forskolin-induced cAMP formations, while mGluR3 and mGluR4 have no known function (Tanabe et al., 1992). Recently, another mGluR coupled to PI hydrolysis, designated mGluR5, has been cloned (Abe et al., 1992).

Utilizing an antiserum generated against peptides from the mGluR1 amino acid sequence and four oligonucleotides derived from the mGluR1 cDNA that specifically recognize mGluR1α and mGluR1β, we have conducted immunohistochemical and *in situ* hybridization localization of mGluR1 protein and mRNA, respectively. We now report a striking contrast in the brain localizations of mGluR1 compared to PI turnover and inositol 1,4,5-trisphosphate receptor (IP_3R) protein and mRNA.

Materials and Methods

Materials. The Vectastain immunohistochemistry kit was purchased from Vector. ^{3}H-cytidine (27.8 Ci/mmol) was obtained from New England Nuclear/Du Pont. All other materials were purchased from Sigma, unless otherwise specified.

Preparation of anti-mGluR1 antiserum. A synthetic peptide based on amino acids 141–154 of mGluR1 protein (Masu et al., 1991) was made and conjugated to bovine serum albumin (BSA). To ensure selective coupling through one of the carboxyl terminal lysine residues, the amino terminus of the peptide was first blocked by reaction of the peptide at pH 7.4 with a twofold molar excess of citraconic anhydride for 3 hr at

Received July 6, 1992; revised Oct. 26, 1992; accepted Nov. 13, 1992.

This work was supported by U.S. Public Health Service Grant MH-18501, Research Scientist Award DA-00074 to S.H.S., a grant from the International Life Sciences Institute, and a gift of the Bristol-Myers-Squibb Company, Postdoctoral Fellowship MH-09953 to A.H.S., Predoctoral Fellowship MH-1001702 to C.E.G., and Training Grant GM-07309 to P.M.H. M.F. is supported in part by FCAR of Quebec, Canada. T.M.D. is a Pfizer Postdoctoral Fellow and is supported by the American Academy of Neurology and the French Foundation for Alzheimer's Research, the Dana Foundation, and U.S. Public Health Service CIDA NS 01578-01.

Correspondence should be addressed to Solomon H. Snyder, Department of Neuroscience, The Johns Hopkins University School of Medicine, 725 North Wolfe Street, Baltimore, MD 21205.

room temperature. BSA was then added to the peptide, to a ratio of approximately 1 BSA molecule per 10 peptide molecules, followed by addition of glutaraldehyde (final concentration, 0.1%) for 1 hr at room temperature. The conjugation reaction was stopped by incubation with excess glycine for 1 hr at room temperature. The conjugate was dialyzed first against 100 mM sodium acetate, pH 4.2, for 5 hr and then against phosphate-buffered saline (PBS) overnight. Antiserum was raised in rabbits injected with the above BSA-conjugated peptide (Cocalico Biologicals, Inc., Reamstown, PA).

Antiserum solution was purified at three steps. First, it was adsorbed overnight, at 4°C, with an affinity matrix consisting of proteins extracted from crude brain membrane using high pH (NaOH extract) and immobilized on cyanogen bromide (CNBr)-activated Sepharose. Preliminary results showed that the mGluR1 protein adheres to a heparin–agarose column (A. H. Sharp, T. M. Dawson, and S. H. Snyder, unpublished observations). Thus, the antiserum solution was further absorbed with an affinity matrix consisting of Triton X-100–solubilized cerebellar membranes that had been passed through a heparin–agarose column before immobilization on CNBr-activated Sepharose. Finally, it was affinity purified using a column consisting of an ovalbumin–mGluR1 peptide conjugate immobilized on CNBr-activated Sepharose, batchwise, overnight at 4°C. The antiserum was eluted from the column with 4 M $MgCl_2$, dialyzed first against PBS and then against PBS containing 20% sucrose, and stored in small aliquots at −70°C until use. IP_3R goat affinity-purified antiserum was produced as described previously (Peng et al., 1991; Sharp et al., 1993).

Western blot analysis. Particulate fractions from different brain regions were prepared in 50 mM Tris HCl buffer containing 1 mM EDTA, 0.5 nM phenylmethysulfonyl fluoride, and 1 mM benzamidine. Proteins (150 μg per lane) were separated on a 7.5% SDS polyacrylamide gel, transferred to Immobilon-P membranes (Millipore), and probed with affinity-purified antibody (1:100) overnight. Blots were then washed and incubated with peroxidase-linked goat anti-rabbit secondary antibody (1:1500; Boehringer Mannheim) for 2 hr at room temperature. Bands were visualized using the chromogen 4-chloro-1-naphthol (Immuno-SELECT). For preadsorption experiments performed on fractions of different brain regions, antibody was preincubated with 20-fold excess of peptide antigen for 24 hr at 4°C.

Immunohistochemistry. Adult male Sprague–Dawley rats were perfused with 2–4% freshly depolymerized paraformaldehyde in 50 mM PBS. Brains were removed and postfixed for 2 hr in 2–4% paraformaldehyde followed by cryoprotection in 20% glycerol overnight. Sections were cut (40 μm) on a sliding microtome and transferred to 50 mM Tris HCl–buffered saline (TBS). They were permeabilized in 0.4% Triton X-100 for 30 min, blocked in 10% normal goat serum for 1 hr, and incubated in primary affinity-purified mGluR1 antibody (1:1000) or affinity-purified IP_3R antibody (1:1000) (Peng et al., 1991) overnight. Immunostaining was visualized with an avidin–biotin kit (Vectastain ABC Kit) in which diaminobenzidine was the chromogen.

In situ *hybridization.* A pool of four antisense oligonucleotide probes, complementary to nucleotides 1779–1827, 2067–2103, 2181–2229, and 2472–2520 of the cloned mGluR1 cDNA (Masu et al., 1991), and a pool of three complementary oligonucleotide probes to nucleotides 1077–1125, 327–375, and 1452–1500 of the cloned IP_3R cDNA (Nordquist et al, 1988), were end labeled with ^{35}S-γ-ATP and terminal transferase (Bethesda Research Labs). *In situ* hybridization was carried out exactly as described previously (Ross et al., 1989). Briefly, 12-μm-thick brain sections were dehydrated, defatted, and then incubated with 1 × 10^6 cpm probe per 100 μl formamide hybridization buffer (50% formamide, 1 × Denhardt's solution, 10 mM sodium phosphate pH 7.4, 1 mM EDTA, 100 μg/ml salmon sperm DNA, 100 μg/ml tRNA, 10% dextran sulfate, and 10 mM dithiothreitol) over 24 hr at 37°C. Sections were washed first for 15 min at room temperature and then for 1 hr at 55°C in 1 × saline–sodium citrate buffer containing 0.1% β-mercaptoethanol, briefly dipped in H_2O, and dried. Sections were exposed to Beta-Max film (Amersham) or dipped in Kodak NTB2 emulsion (1:1 with H_2O) and allowed to expose for 1–3 weeks at −70°C. Each individual probe gave identical distributions in the brain to other probes in that pool (data not shown).

Electron microscopy. Adult male Long–Evans Hooded and Sprague–Dawley rats (150–300 gm) were used for immunoelectron microscopic analysis. The animals were given a lethal dose of anesthetic and perfused transcardially with cold, oxygenated (95% O_2, 5% CO_2) artificial cerebrospinal fluid (126 mM NaCl, 2.5 mM KCl, 1.25 mM NaH_2PO_4, 2 mM $MgSO_4$, 26 mM $NaHCO_3$) and immediately followed by 500 ml of cold fixative [4% paraformaldehyde, 0.05% glutaraldehyde in 0.1 M phosphate buffer (PB) pH 7.4]. The brains were removed and placed into the fixative solution overnight before being cut into blocks and sectioned to 50 μm on a vibrating microtome. The sections containing the striatum were placed into a cryoprotecting solution consisting of 25% sucrose and 5% glycerol in 50 mM PB (pH 7.4). Once the sections had sunk in the cryoprotectant, they were freeze thawed in isopentane that had been chilled in liquid nitrogen.

The immunohistochemical procedure was carried out as above. Sections were then rinsed in phosphate buffer (pH 7.4) and postfixed in 1% osmium tetroxide for 30 min. They were then briefly rinsed in TBS before being incubated in a 2% uranyl acetate solution (aq) for 45–60 min. Following this, they were dehydrated through a graded series of alcohol, followed by propylene oxide prior to embedding in resin (Durcupan ACM, Fluka). Sections were placed in Durcopan overnight before being flat embedded between two silicon-coated (Sigmacote, Sigma) glass slides. The resin was then polymerized at 60°C for 48 hr. After light microscopic analysis, areas of the striatal matrix regions were selected and cut out from the slides and reembedded in blocks for further sectioning. These blocks were then sectioned for electron microscopy on a ultramicrotome and collected on either copper mesh grids or Pioloform-coated copper slot grids. The ultrathin sections were then examined with a JEOL 100S electron microscope, with some grids being stained with lead citrate.

Phosphoinositide (PI) turnover and imaging. Regions of rat brain corresponding to those areas in the regional Western blot analysis were rapidly dissected and cross-chopped into 400 μm pieces of tissue. The cross-chopped tissue was first allowed to recover for 30 min in Krebs–bicarbonate buffer followed by incubating (50 μl of gravity-picked tissue) in 250 μl of Krebs–bicarbonate buffer containing 0.1 μCi/ml ^3H-cytidine (Du Pont/New England Nuclear; 27.8 Ci/mmol) in an interface chamber (95% O_2, 5% CO_2) at 37°C. LiCl (final concentration, 5 mM) was subsequently added followed 10 min later by 300 μM *trans*-1-aminocyclopentane-1,3-dicarboxylate (t-ACPD). After 1 hr of incubation at 37°C, the reaction was stopped on ice, membranes were lipid extracted, and the amount of radioactivity, that is, ^3H-cytidine diphosphate diacylglycerol (^3H-CDP-DAG) accumulation, was determined using a scintillation counter (Godfrey, 1989).

The steps in PI imaging are similar and were carried out exactly as described (Hwang et al., 1990a). Briefly, rat brain slices (400 μm) of olfactory bulb, hippocampus, or cerebellum were allowed to recover for 1 hr at 20°C in an interface chamber (95% O_2, 5% CO_2). They were prelabeled on Whatman filter paper circles (2.1 cm in diameter) that were immersed in 0.1 ml of Krebs–bicarbonate buffer (on upside-down covers of 24-well tissue culture plates) containing 4.0 μCi/ml ^3H-cytidine (Du Pont/New England Nuclear; 27.8 Ci/mmol), 1 μg/ml actinomycin (Boehringer Mannheim), and 50 μM hydroxyurea (Sigma) for 1 hr at 30°C. LiCl (5 mM final concentration) was added beneath the Whatman filter paper with tissue on top 10 min prior to addition of 100–300 μM t-ACPD in order to allow even diffusion of LiCl. Following 50–60 min of incubation at 37°C, sections were transferred to plastic molds and embedded in 0.C.T. medium (Tissue-Tek). Frozen sections were cut (16 μm) on gelatin-coated glass slides, treated in wash buffer (50 mM Tris HCl pH 4.2, 2 mM EDTA, 10 mM LiCl, 1 mM cytidine, 3% polyethylene glycol, 0.005% saponin, 20 μg/ml each of RNase A and DNase I) for 2–5 min at 37°C, quickly dried, and apposed to film (Hyperfilm-^3H, Amersham) or Kodak NTB emulsion-coated coverslips for 2–4 weeks.

Results

mGluR1 protein levels and ACPD-stimulated PI turnover differ in brain regions. A rabbit polyclonal antiserum corresponding to the peptides 141–154 of the N-terminal region of mGluR1 (Masu et al., 1991) was developed. It recognizes mGluR1 by Western blot analysis. Interestingly, two immunoreactive bands are identified at about 140 kDa and 100 kDa, in all brain regions (Fig. 1). Preadsorption of the antiserum with excess peptide antigen completely eliminated staining, in cerebellum and other brain regions (data not shown) (Fig. 1). These bands correspond to the predicted molecular weights of the cloned mGluR1α and mGluR1β, respectively (Tanabe et al., 1992). The relative abundance of mGluR1α and mGluR1β differ in brain regions, with

mGluR1α predominating in the cerebellum and olfactory bulb and mGluR1β as the major form in other areas.

To assess the relationship between the amount of mGluR1 immunoreactivity and glutamate-mediated PI turnover, we measured t-ACPD (a selective ligand for the mGluR1)-stimulated PI turnover in various brain regions and conducted Western blot analysis of mGluR1 protein in the same brain regions (Fig. 1). We detect t-ACPD–elicited PI turnover in all regions containing mGluR1 protein. However, the relative intensity of mGluR1 staining is dissociated from the relative amount of t-ACPD–stimulated PI turnover. For instance, highest levels of mGluR1 protein are found in the cerebellum, which contains only moderate levels of t-ACPD–stimulated PI turnover (Fig. 1).

mGluR1 localizations differ from those of IP_3R mRNA and protein. The PI cycle involves receptor-mediated stimulation of phospholipase C (PLC) activity generating diacylglycerol (DAG), which stimulates protein kinase C (PKC) activity, and IP_3, which binds to the IP_3R to evoke calcium release (Berridge and Irvine, 1989; Ferris and Snyder, 1992). Localizations for protein and mRNA of PLC (Gerfen et al., 1988; Ross et al., 1989), PKC (Worley et al., 1986a,b, 1987; Huang et al., 1988; Saito et al., 1988; Yoshihara et al., 1991), and IP_3R (Worley et al., 1989; Nakagawa et al., 1991a,b; Nakanishi et al., 1991) are closely similar, though not identical (Worley et al., 1987). There are also some differences in the disposition of subtypes of PLC (Gerfen et al., 1988; Ross et al., 1989) and PKC (Yoshihara et al., 1991). Only one major form of IP_3R has been identified by protein purification and molecular cloning, though alternatively spliced forms of this IP_3R exist (Danoff et al., 1991; Nakagawa et al., 1991a,b) and recently quantitatively minor forms of distinct subtypes of IP_3R derived from different genes have been identified (Südhof et al., 1991; Ross et al., 1992). Because the distribution of the quantitatively major, first isolated form of the IP_3R resembles other markers of the PI cycle, we have compared its localization to that of mGluR1. If mGluR1 is coupled to PI turnover, one would anticipate close similarities between the distribution of mGluR1 and IP_3R.

In numerous areas, the localizations of mGluR1 and IP_3R protein and mRNA differ strikingly (Figs. 2–5, Table 1; see also Fig. 8). For instance, in the cerebellum IP_3R mRNA and protein are exclusively localized to Purkinje cells and their processes, while mGluR1 occurs both in Purkinje cells and granule cells. mGluR1 mRNA is highly concentrated in deep cerebellar nuclei that are devoid of IP_3R mRNA (Fig. 2). IP_3R protein occurs in Purkinje cell terminals synapsing upon deep cerebellar nuclei, whereas mGluR1 protein is apparent within perikarya of these nuclei (data not shown).

IP_3R protein and mRNA are concentrated within pyramidal cells of all regions and lamina of the cerebral cortex (Figs. 2–5). In contrast, mGluR1 mRNA is confined to occasional nonpyramidal neurons throughout the cortex (Fig. 5*C*). Substantial mGluR1 protein is evident within the cortical neuropil, apparently reflecting terminal patterns that may arise from the thalamus, where mGluR1 mRNA and protein levels are high.

In the hippocampus, IP_3R and mGluR1 protein and mRNA (Figs. 2–4, 6) display notably reciprocal localizations. IP_3R is concentrated in a dense band comprising the CA1 pyramidal layer with much lower levels in CA3, whereas mGluR1 is enriched in CA3 with low levels in CA1. mGluR1 immunoreactivity is concentrated in fine fibers in the stratum oriens of CA1 and the subiculum, where staining for IP_3R is minimal (Fig. 6,

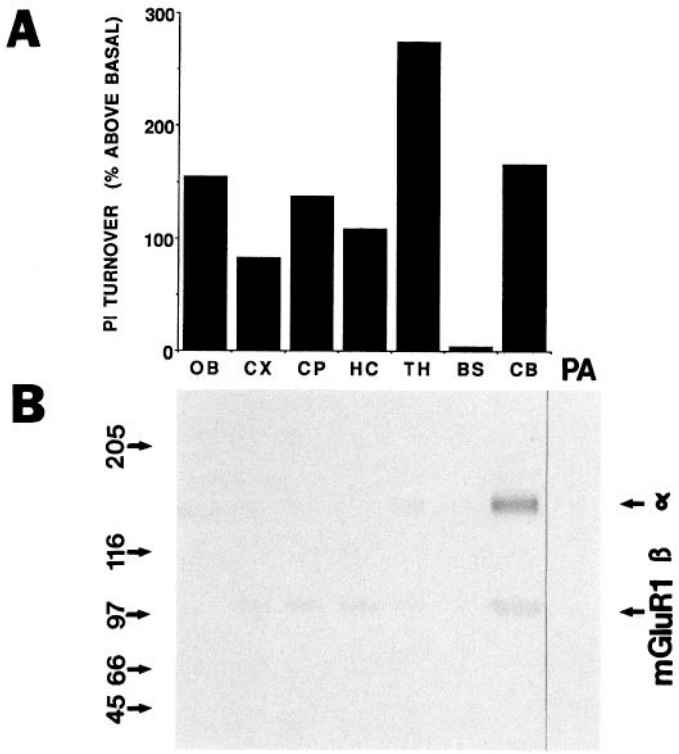

Figure 1. Regional distribution of PI turnover and mGluR1 protein in brain. PI turnover (*A*) and Western blot analysis (*B*) experiments were carried out as described in Materials and Methods. t-ACPD–stimulated PI turnover represents the mean of two to four experiments performed in triplicate in which the results varied less than 10%. Control levels of ^{3}H-CDP-DAG were consistently approximately 100 cpm/50 mg tissue. Preadsorption (*PA*) with excess peptide completely attenuates the cerebellar immunoreactive band observed on Western blot analysis. *OB*, olfactory bulb; *CX*, cortex; *CP*, caudate-putamen; *HC*, hippocampus; *TH*, thalamus–hypothalamus; *BS*, brainstem; *CB*, cerebellum.

Table 1; see also Fig. 9). The molecular layer of the dentate gyrus displays very low levels of IP_3R but high levels of mGluR1. In contrast, the granule cell layer of dentate gyrus exhibits high IP_3R and low mGluR1 levels.

The olfactory bulb provides further evidence for a dissociation between mGluR1 and IP_3R mRNA and protein (Figs. 2–4, 7; Table 1; see also Fig. 9). Substantial levels of mGluR1 protein occur in the glomeruli, external plexiform, and mitral cells of the olfactory bulb, while IP_3R is concentrated within the periglomerular and granule cells with moderate levels in tufted cells (Fig. 7*A,B*).

Divergent patterns in the thalamus (Figs. 2–4, Table 1) are evident for mGluR1 and IP_3R mRNA and protein. In contrast to high mGluR1 levels, IP_3R levels are much lower in most of the thalamus. The anterior dorsal thalamic nucleus contains abundant mGluR1 but no IP_3R at all. The anterior ventral nucleus and the ventral lateral posterior nucleus are enriched in mGluR1 with low levels of IP_3R. The medial and lateral geniculate nuclei contain high levels of mGluR1, but only low to moderate levels of IP_3R (Fig. 4). Similarly, the gelatinosum nucleus and subthalamic nucleus are enriched in mGluR1 but lack substantial staining for IP_3R. In the hypothalamus, dramatic reciprocity of mGluR1 and IP_3R is evident in the lateral hypothalamic nucleus with high levels of mGluR1 but no IP_3R (Figs. 4, 7*E,F*). By contrast, the dorsal medial hypothalamic

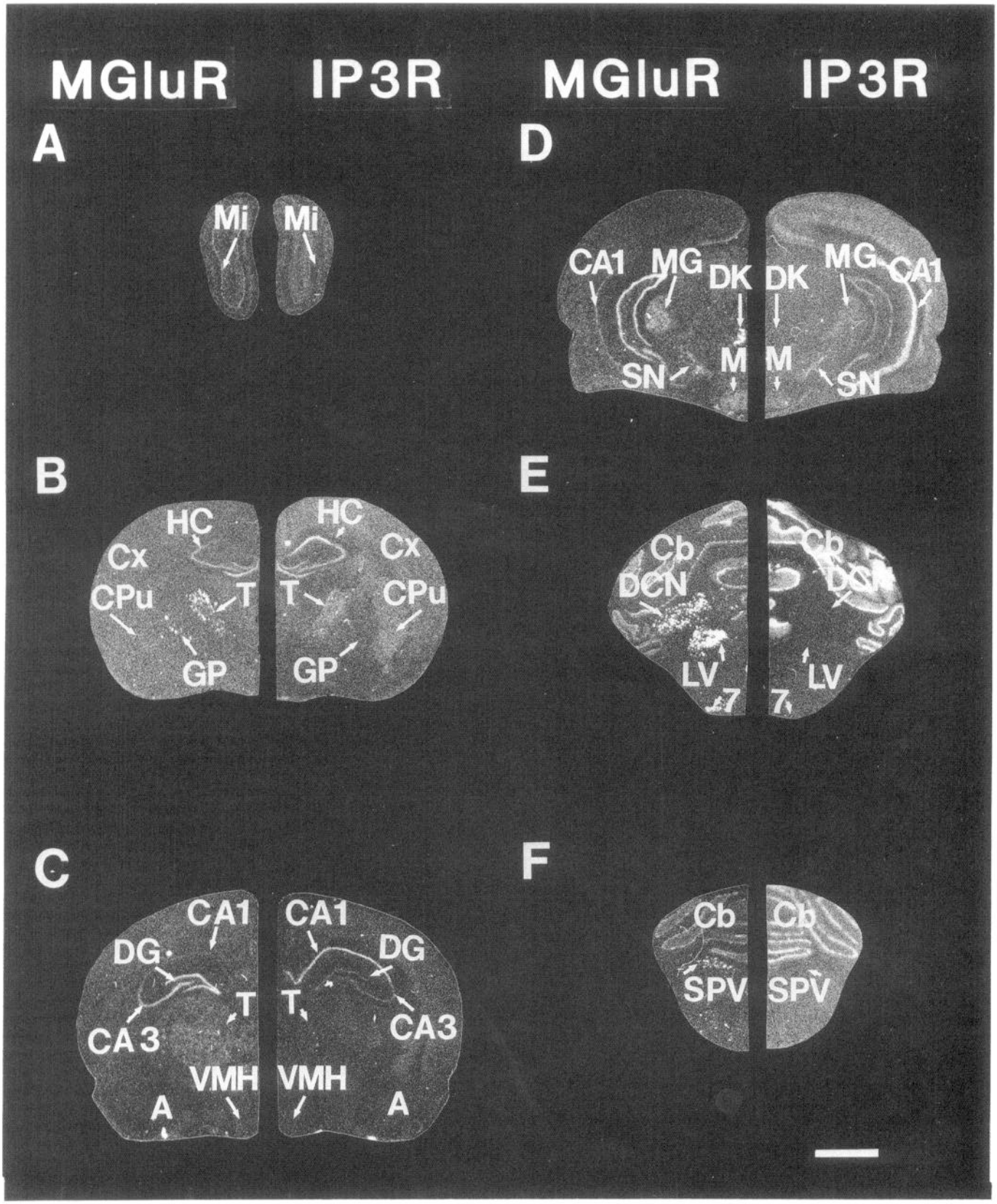

Figure 2. Comparison of the localization of mGluR1 (α and β) and IP_3R mRNAs. Pairs of adjacent thin (12 μm) sections of rat brain were processed for *in situ* hybridizations with ^{35}S-labeled oligonucleotides specific for mGluR1 (*left*) and IP_3R (*right*) cDNAs. Labeled structures appear *white* in these dark-field images. The relatively higher level of mGluR1 versus IP_3R labeling is evident in the mitral layer (*Mi*) of the olfactory bulb, *CA3* region of hippocampus (*HC*), dentate gyrus (*DG*), globus pallidus (*GP*), thalamic nuclei (*T*) including medial geniculate nucleus (*MG*), and in the mammillary bodies (*M*). mGluR1 labeling also occurs in apparent absence of IP_3R labeling in the Darkshevich's nucleus (*DK*), deep cerebellar nuclei (*DCN*), lateral vestibular nucleus (*LV*), facial nucleus (*7*), and spinal motor nucleus of the trigeminal nerve (*SPV*). Conversely, higher amounts of IP_3R labeling appear in cortex (*Cx*), caudate-putamen (*CPu*), *CA1* region of hippocampus, upper layer (pars compacta) of substantia nigra (*SN*), and Purkinje layer of cerebellum (*Cb*). Amygdala (*A*) and ventral medial nucleus of hypothalamus (*VMH*) contains low levels of labeling for both mGluR1 and IP_3R. Scale bar, 100 μm.

nucleus displays abundant IP_3R with negligible mGluR1 (data not shown).

The striatum possesses low levels of mGluR1 mRNA but high levels of IP_3R mRNA (Fig. 2). However, both mGluR1 and IP_3R proteins are abundant (Figs. 3, 4). IP_3R is primarily localized to perikarya and dendrites of medium spiny neurons (Figs. 3, 4, 8) and is enriched within the striosomal compartment (Fotuhi et al., 1991). In contrast, mGluR1 is enriched in the presynaptic terminal fields in neuropil within the matrix compartment, although occasional postsynaptic neurons stain for mGluR1 (Figs. 3, 8, and data not shown). The nearby islands of Calleja are enriched in mGluR1 with no IP_3R, whereas the surrounding olfactory tubercle contains abundant IP_3R but is devoid of mGluR1 (Figs. 4, 7*C,D*).

The substantia nigra pars compacta contains low mGluR1 but high IP_3R mRNA and protein (Figs. 2–4) in neurons with a pattern characteristic of dopamine-containing cell bodies. Within the substantia nigra pars reticulata, both mGluR1 mRNA and protein are present. In contrast, IP_3R mRNA is absent in pars reticulata, but IP_3R protein is enriched, apparently reflecting terminal patterns from striatal projection neurons.

In the brainstem and midbrain regions (Figs. 2–4, Table 1) striking differences in mGluR1 and IP_3R dispositions are evident in the nucleus of Darkshevich, the lateral vestibular nuclei, the red nucleus, and the cranial nerve nuclei. mGluR1 mRNA and protein are highly enriched in these structures, but IP_3R mRNA and protein are virtually absent (Figs. 2*E,F*; 4). The superior colliculus contains high levels of mGluR1 protein, but only moderate levels of IP_3R. In contrast, the pontine nuclei are enriched in IP_3R but low in mGluR1 (Fig. 3).

Electron microscopy reveals dissociation of mGluR1 and IP_3R at the ultrastructural level. In the striatum, mGluR1 is primarily localized to presynaptic terminals (Fig. 8), although occasional postsynaptic densities do occur (data not shown). In contrast, IP_3R immunoreactivity is predominantly enriched in all postsynaptic structures. These include somata, dendritic shafts, and spines (Fig. 8).

Dissociation of mGluR1 protein from IP_3R protein and t-ACPD–stimulated PI turnover. To explore further the dissociation of mGluR1 and IP_3R proteins, we compared the anatomical distribution of mGluR1 and IP_3R proteins with t-ACPD–stimulated PI turnover in tissue slices (Fig. 9). In the olfactory bulb, both t-ACPD–stimulated PI turnover and mGluR1 immunoreactivity are concentrated within the glomeruli. In contrast, IP_3R is concentrated in periglomerular cells (Figs. 7, 9). The hippocampus displays striking differences between t-ACPD–elicited PI turnover, mGluR1, and IP_3R protein (Fig. 9). Both t-ACPD–stimulated PI turnover and mGluR1 are enriched in CA3 with low levels of IP_3R. In contrast, mGluR1 protein is abundant within the molecular layer of the dentate gyrus, where there are low amounts of IP_3R and t-ACPD–stimulated PI turnover. The CA1 region contains low levels of t-ACPD–stimulated PI turnover, which might reflect mGluR1 within the stratum oriens. In the cerebellum all three markers are enriched within the molecular layer. However, there is virtually no t-ACPD–stimulated PI turnover in the deep cerebellar nuclei, where both IP_3R and mGluR1 proteins are present in high concentrations.

Discussion

mGluR1 is distributed distinctly throughout all regions of the brain, with highest levels in the olfactory bulb, CA3 and the dentate gyrus of the hippocampal formation, the thalamus, lateral hypothalamus, cranial nuclei of the brainstem, and the cerebellum. mGluR1 immunoreactivity in some areas (e.g., lateral hypothalamus) is limited to neuronal perikarya, while in other areas it is enriched in the neuropil (e.g., cerebral cortex).

Our antibody apparently recognizes both the long and short forms of mGluR1, mGluR1α, and mGluR1β, respectively. It is not known whether mGluR1β is a functional receptor (Tanabe et al., 1992), but the identification of a protein of appropriate molecular weight (100 kDa) by our antibody suggests that mGluR1β is expressed in several brain regions. The anatomical distribution of our antibody is much more extensive, although completely inclusive of the distribution of an antibody specific for mGluR1α (Martin et al., 1992). Presumably, the immunostaining shown here represents both mGluR1α and mGluR1β as staining is completely blocked by preadsorption with excess peptide. Interestingly, Western blot analysis reveals differences between the distribution of mGluR1α and mGluR1β. mGluR1α is present in the olfactory bulb and is present in high amounts in the thalamus, and cerebellum, while mGluR1β is enriched in the cortex, caudate-putamen, and hippocampus as well as in the olfactory bulb, thalamus, and cerebellum (Fig. 1). mGluR1β may be located primarily presynaptically, as our electron microscopy in the striatum shows a predominant presynaptic labeling pattern and the Western blot analysis demonstrates that the striatum contains very low levels of mGluR1α. Consistent with mGluR1 immunoreactivity primarily limited to presyn-

→

Figure 3. Immunohistochemical localization of mGluR1 and IP_3R proteins in sagittal brain sections. Adjacent thick (40 μm) rat sagittal brain sections were stained with affinity-purified antibodies against mGluR1 (α and β) (*A*) and IP_3R (*B*). *C*, Preadsorption (*PA*) of antibodies against mGluR1 with its respective antigen completely abolishes immunostaining; similar results were obtained with the IP_3R antibody (data not shown). Immunoreactive structures appear *white* in these dark-field images. Areas high in mGluR1 immunoreactivity but low in IP_3R immunoreactivity include olfactory bulb (*OB*), *CA3* of the hippocampus, dentate gyrus (*DG*), thalamus (*T*), granular layer of cerebellum (*Cb*), superior colliculus (*SC*), and lateral hypothalamus (*LH*). Areas low in mGluR1 and high in IP_3R immunostaining include the anterior olfactory nucleus (*AO*), olfactory tubercle (*Tu*), pyramidal cell layer of cortex (*Cx*), caudate-putamen (*CP*), and pontine nucleus (*Pn*). *SN*, substantia nigra. Scale bar, 2.5 mm.

Figure 4. Contrasting localization of mGluR1 and IP_3R immunoreactivity in coronal brain sections. Pairs of adjacent thick (40 μm) coronal rat brain sections were immunohistochemically processed with affinity-purified mGluR1 (*left*) and IP_3R (*right*) antibodies. Positive staining appears *white* in these dark-field images. The contrasting distributions of these two proteins revealed by *in situ* hybridization in Figure 2 is more clearly apparent in these immunostained sections. Much higher amounts of mGluR1 staining are present in the olfactory bulb (*OB*) and in the following thalamic nuclei: anterodorsal (*AD*), anteroventral (*AV*), ventrolateral posterior (*VPL*), medial geniculate (*MG*), and nucleus gelatinosum (*G*). The lateral hypothalamus (*LH*), islands of Calleja (*ICj*), mammillary bodies (*M*), and nucleus of Darkshevich (*DK*) also exhibit more mGluR1 than IP_3R immunoreactivity. Similarly, in the brainstem, many of the cranial nuclei including the motor nucleus of the trigeminal nerve (*5*) as well as the substantia gelatinosa and ventral horn of spinal cord (*Sc*) contain higher amounts of mGluR1 immunoreactivity. Areas with higher IP_3R immunoreactivity depicted in these sections include the internal capsule (*ic*), *CA1* of hippocampus, pars reticulata (the lower portion) of substantia nigra (*SN*), and Purkinje cell layer of cerebellum (*Cb*). *DG*, dentate gyrus; *CP*, caudate-putamen; *Cx*, cortex. Scale bar, 2.5 mm.

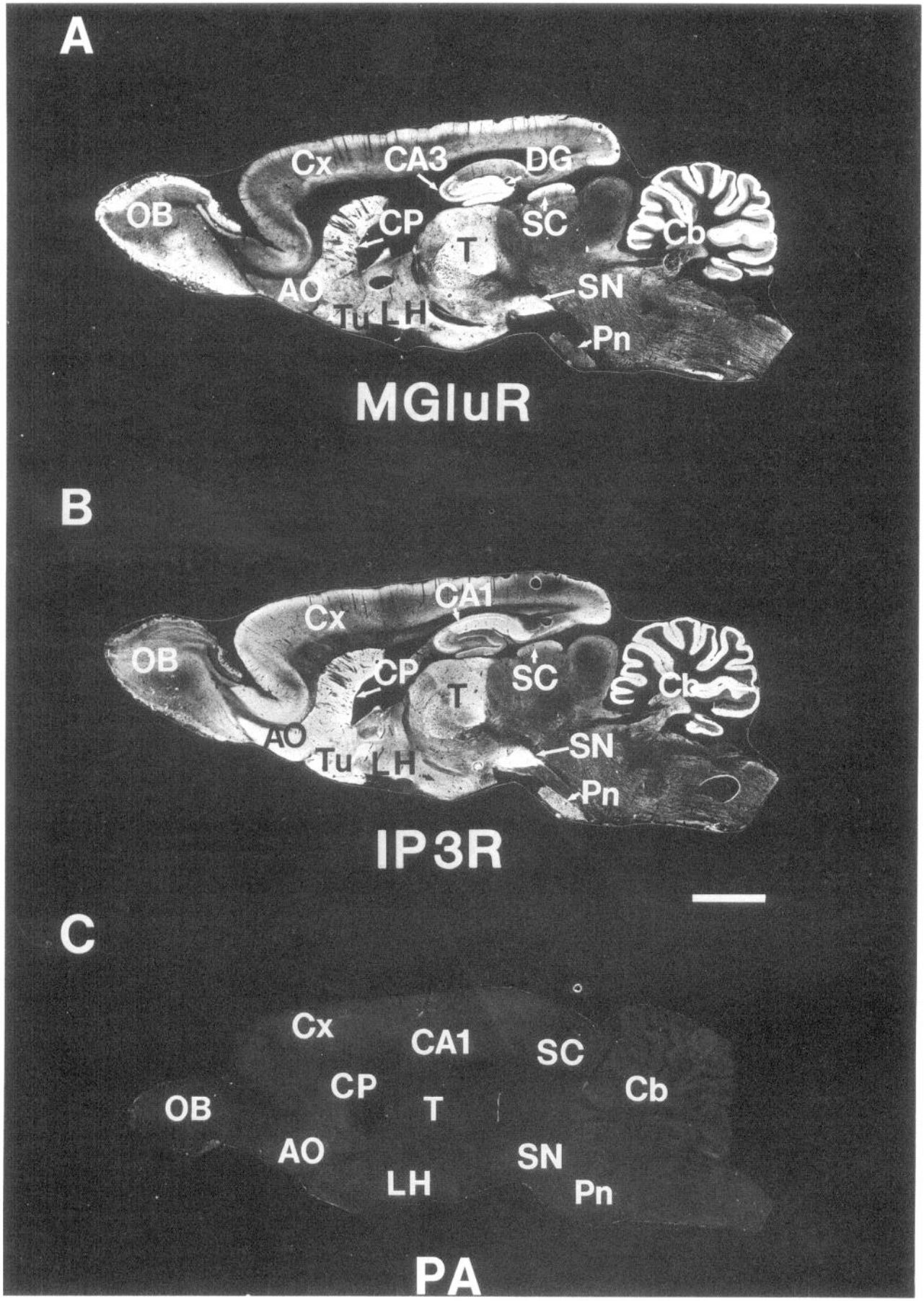
A
Cx
CA3
DG
OB
CP
SC
Cb
T
AO
SN
Tu
LH
Pn
MGluR
B
CA1
Cx
OB
CP
SC
Cb
T
AO
SN
Tu
LH
Pn
IP3R
C
Cx
CA1
SC
CP
Cb
OB
T
AO
SN
LH
Pn
PA

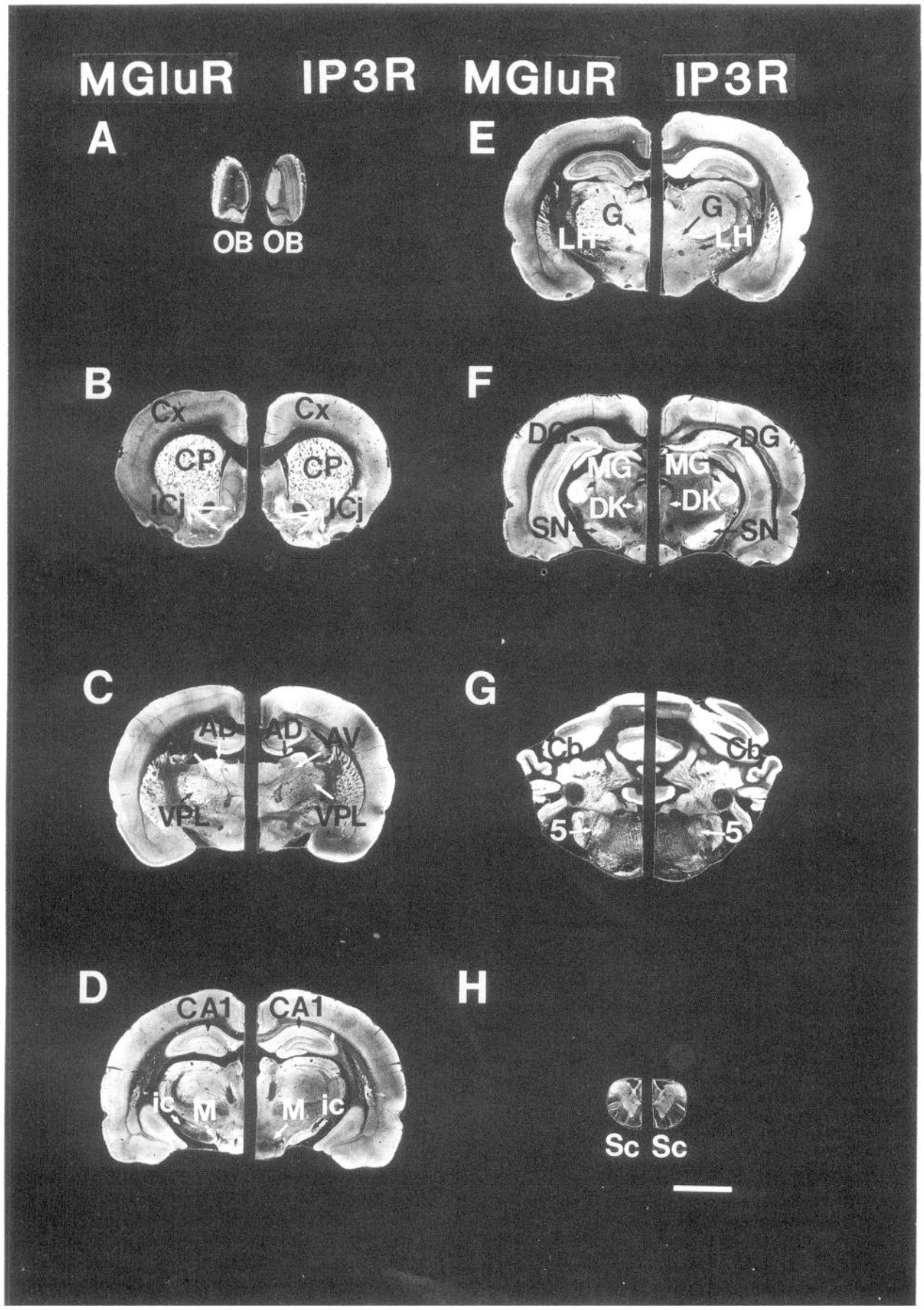
MGluR
IP3R
MGluR
IP3R
A
OB OB
E
G
LH
G
LH
B
Cx
CP
ICj
Cx
CP
ICj
F
DG
MG
DK
SN
DG
MG
DK
SN
C
AD
AD
AV
VPL
VPL
G
Cb
Cb
5
5
D
CA1
CA1
ic
M
M
ic
H
Sc Sc

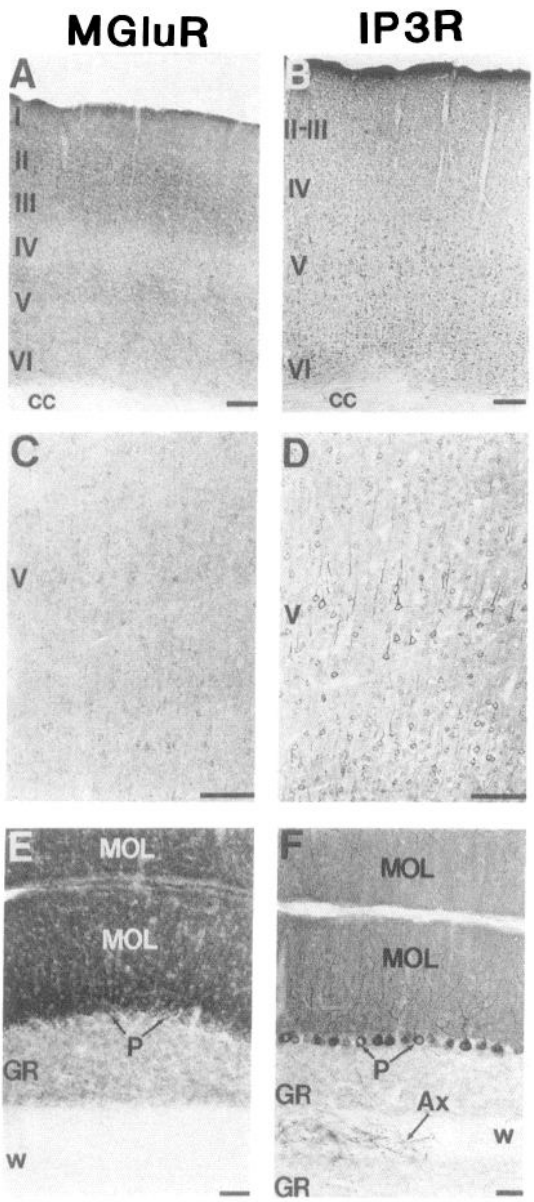

Figure 5. Contrasting localizations of mGluR1 and IP_3R immunoreactivity in the cerebral cortex and cerebellum. Adjacent sections were immunostained with mGluR1 (*left*) and IP_3R (*right*) antibodies. mGluR1 immunostaining is mostly in the neuropil as well as in the cell bodies of nonpyramidal cells enriched in layers II, III, V, and VI (*A, C*). IP_3R immunostaining differs from that of mGluR1 in being more concentrated in the cell bodies of pyramidal cells (*B, D*). Neither antibody stains glia, as the corpus callosum (*cc*) appears blank. In the cerebellum (*E, F*), Purkinje cell bodies (*P*) and their dendrites in the molecular layer (*MOL*) both contain high levels of mGluR1 and IP_3R immunoreactivity, though with somewhat different patterns. The granule cells (*GR*), on the other hand, are enriched in mGluR1 but lack IP_3R. As in the corpus callosum, the white matter (*w*) of cerebellum is devoid of immunoreactivity. Axonal staining (*Ax*) appears in the white matter for IP_3R but not for mGluR1. Scale bars, 100 μm.

aptic terminals in the caudate-putamen (Fig. 8), electrophysiological studies indicate that t-ACPD decreases synaptic excitation via presynaptic mechanisms, perhaps through inhibition of glutamate release (Baskys and Malenka, 1991; Lovinger, 1991). The ultrastructural localization of mGluR1 in the striatum is interesting in light of the fact the PI-linked glutamate receptors were first identified in cultured striatal neurons (Sladeczek et al., 1985). Presumably these receptors are postsynaptic. Perhaps the ultrastructural localization of the novel PI-linked glutamate receptor (mGluR5) will be postsynaptic in striatum.

Table 1. Brain distributions of mGluRl, IP_3R, and PKC

	mGluRl	IP_3R	PKC
Olfactory bulb			
External plexiform layer	4	1	4
Mitral cell layer	3	1	1
Anterior olfactory n.	1	4	5
Basal ganglia			
Caudate-putamen	3	4	4
Globus pallidus	3	1	1
Subthalamic n.	4	0	0
Hippocampal formation			
Stratum oriens CA1	4	2	5
Stratum oriens CA3	4	2	4
Stratum radiatum CA1	0	4	5
Stratum radiatum CA3	2	1	3
Dentate gyrus			
Granular cell layer	1	3	2
Molecular cell layer	4	1	4
Thalamus			
Anterodorsal n.	5	0	2
Anteroventral n.	4	1	3
Medial geniculate	4	2	3
Gelatinosum n.	3	1	1
Hypothalamus			
Lateral n.	4	0	2
Mammillary n.	4	2	1
Cerebral cortex			
Pyramidal cells	0	4	4
Nonpyramidal cells	3	1	1
Cerebellum			
Molecular layer	5	5	5
Granular cell layer	3	0	1
Deep cerebellar n.	3	2	3
Midbrain			
Superior colliculus	4	3	3
Red n.	3	0	0
Substantia nigra	2	4	4
Locus coeruleus	1	3	2
Darkshevich's n.	5	0	0
Cranial n.			
Vestibular n.	4	1	1
Motor n. of trigeminal	3	1	1
Facial n.	3	1	1

The distribution of mGluRl corresponds to that of IP_3R in some areas and to that of PKC in other areas. In some areas enriched in mGluRl, high amounts of both IP_3R and PKC are present, yet in other areas neither IP_3R nor PKC are detected. The values in mGluRl and IP_3R columns are from the immunohistochemical stainings presented here and range from lowest (0) to highest (5) based on visual inspection of the average of six sets of immunostaining experiments. The values for PKC are from Worley et al. (1986a,b, 1987; and M. Fotuhi, T. M. Dawson, and S. H. Snyder, unpublished observations).

The present study shows substantial differences between the localizations of mGluR1 and IP_3R mRNA and protein. As mGluR1 is believed to be linked to PI turnover, one might have expected its protein and mRNA to be distributed similarly to IP_3R. Instead, in numerous parts of the brain, we have observed a reciprocal localization of mGluR1 and IP_3R. In some areas, such as the islands of Calleja and anterodorsal nucleus of thal-

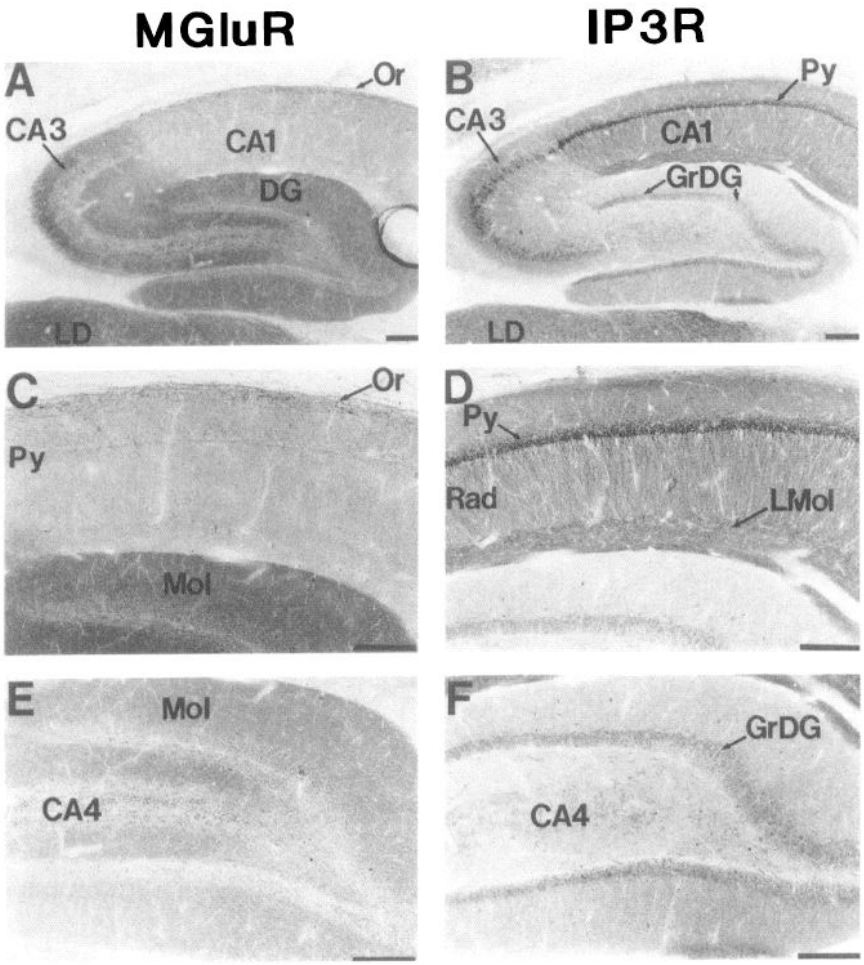

Figure 6. Reciprocal localizations of mGluR1 and IP_3R immunoreactivity in the hippocampal formation. In these bright-field images of an adjacent pair of sections immunostained with mGluR1 (*left*) and IP_3R (*right*) antibodies, *dark areas* represent positive staining. Stratum oriens of *CA1* and *CA3* (*Or* in *A* and *C*) and *CA4* contain an abundance of mGluR1-positive cells and processes in the absence of any appreciable IP_3R immunostaining. The reverse occurs for pyramidal (*Py*) cells and processes in stratum radiatum (*Rad*) of CA1, the lacunosum molecular (*LMol*), and granule cells of dentate gyrus (*GrDG*). *LD*, lateral dorsal nucleus of thalamus; *DG*, dentate gyrus; *Mol*, molecular layer of dentate gyrus. Scale bars, 100 μm.

amus, we observe high levels of mGluR1 in the complete absence of IP_3R. The PI cycle can be differentiated in terms of subtypes of PLC that have been selectively localized in the brain (Gerfen et al., 1988; Ross et al., 1989). Still, since the various forms of PLC all presumably generate IP_3, one would not anticipate brain areas enriched in mGluR1 but devoid of IP_3R. While other subtypes of IP_3R have been identified, they appear to be of much lower abundance than the form of IP_3R described here (Danoff et al., 1991; Nakagawa et al., 1991a,b; Südhof et al., 1991; Ross et al., 1992). However, the minor subtypes of IP_3R may be concentrated in certain brain regions that more closely parallel the distribution of mGluR1α and β. In such regions of dissociation of mGluR1 from IP_3R, it is conceivable that mGluR acts through the PI cycle primarily to activate PKC. Several areas that are devoid of IP_3R possess high levels of both mGluR1 and PKC (Table 1). Consistent with this possibility, quisqualate, which potently activates mGluR, stimulates a rapid and transient translocation of PKC activity in striatal neurons (Manzoni et al., 1990). In addition, glutamate causes a transient phosphorylation of three PKC substrates in a time scale comparable to DAG production (Scholz and Palfrey, 1991).

Perhaps the distribution of mGluR5 may better fit with IP_3R localizations in some brain regions. The existence of other subtypes of PI-linked mGluR as yet unidentified may also parallel the distribution IP_3R better. For instance, in the molecular cloning studies, cross-hybridized cDNA clones were isolated from a cDNA library prepared from a certain size of mRNA (approximately 3–4 kilonucleotides and greater than 4 kilonucleotides), and it is possible that a different size of cDNA may encode a distinct subtype of PI-linked mGluR. Furthermore, several groups have reported the possible existence of other subtypes of the PI-linked mGluR, such as the ibotenate-preferring mGluR (see Schoepp et al., 1990, for review).

We have also localized PI turnover by autoradiographical localization of ^{3}H-CDP-DAG following the stimulation of mGluR1 by t-ACPD in the presence of ^{3}H-cytidine. ^{3}H-CDP-DAG accumulation is a reliable technique for visualization of PI cycle as it is stoichiometrically linked to agonist-stimulated inositol formation (Godfrey, 1989; Hwang et al., 1990a,b; Kennedy et al., 1990). Similar to contrasting localization between mGluR1 and IP_3R immunoreactivities, there are discrepancies in t-ACPD–stimulated PI turnover, mGluR1, and IP_3R immunoreactivity. For instance, ^{3}H-CDP-DAG accumulation and mGluR1 are high in the external plexiform layer of the olfactory bulb, where minimal amounts of IP_3R are detected (Fig. 9). Moreover, t-ACPD–stimulated PI turnover and IP_3R are low in the molecular layer of the dentate gyrus, where there are high levels of mGluR1 protein. Both these areas contain abundant amounts of PKC, suggesting that the actions of mGluR1 may be mediated through the PKC limb of the PI cycle. We also noted a lack of correlation of mGluR1 protein levels as determined by Western blot analysis and t-ACPD–stimulated PI turnover assessed by ^{3}H-CDP-DAG. Similar results in the level of t-ACPD–stimulated PI turnover in various

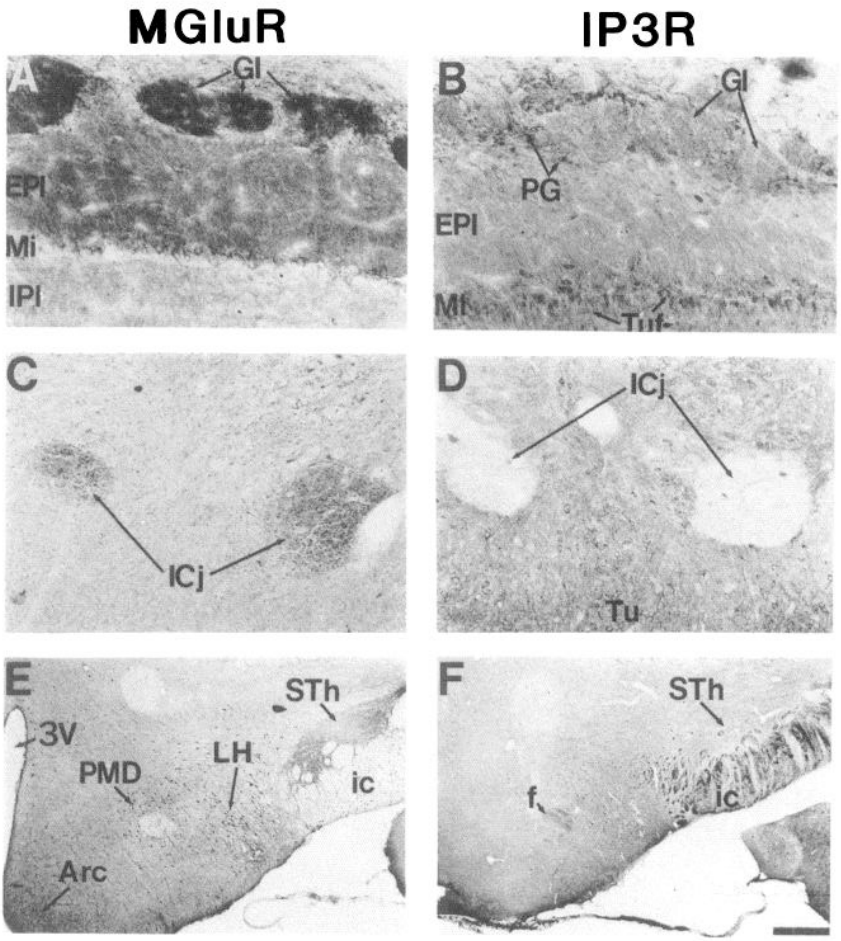

Figure 7. Reciprocal distribution of mGluR and IP_3R immunoreactivity in other brain regions. Pairs of thick (40 μm) rat brain sections were immunostained with mGluR1 (*left*) and IP_3R (*right*) antibodies. Positive staining appears as *dark areas* in these bright-field images. In the olfactory bulb (*A, B*), mGluR1 immunostaining appears dense in the glomeruli (*Gl*), in the external plexiform layer (*EPl*), but low in the internal plexiform layer (*IPl*). In contrast, the IP_3R immunostaining is enriched in periglomeruli cells (*PG*) and tufted cells (*Tuf*) in the mitral cell layer (*Mi*), where mGluR1 protein level is low. In a pair of coronal sections (*C, D*) through rostral striatum, seen at high magnification, islands of Calleja (*ICj*) and olfactory tubercle (*Tu*) contain extremely high and low amounts of mGluR, respectively. The exact opposite occurs for IP_3R immunoreactivity. Similarly, the arcuate nucleus (*Arc*), the lateral hypothalamic nucleus (*LH*), subthalamic nucleus (*STh*), dorsal perimammillary nucleus (*PMD*), fornix (*f*), and internal capsule (*ic*) exhibit reciprocal immunostaining for mGluR and IP_3R proteins. *3V*, third ventricle. Scale bar, 100 μm.

brain regions have been obtained by assessment of ^{3}H-inositol phosphate accumulation, and there is also a marked discrepancy in these levels with the levels of mGluR1 mRNA (Condorelli et al., 1992).

Together, these findings raise the possibility that mGluR1 may act through the PI cycle to activate primarily IP_3R or PKC depending on the relative distribution of the various components. Many other brain regions such as the subthalamic nucleus, red nucleus, and Darkshevich's nucleus are highly enriched in mGluR1 but are devoid of both IP_3R and PKC, suggesting the possibility that mGluR1 may also act through other second messengers. For instance, activation of phospho-

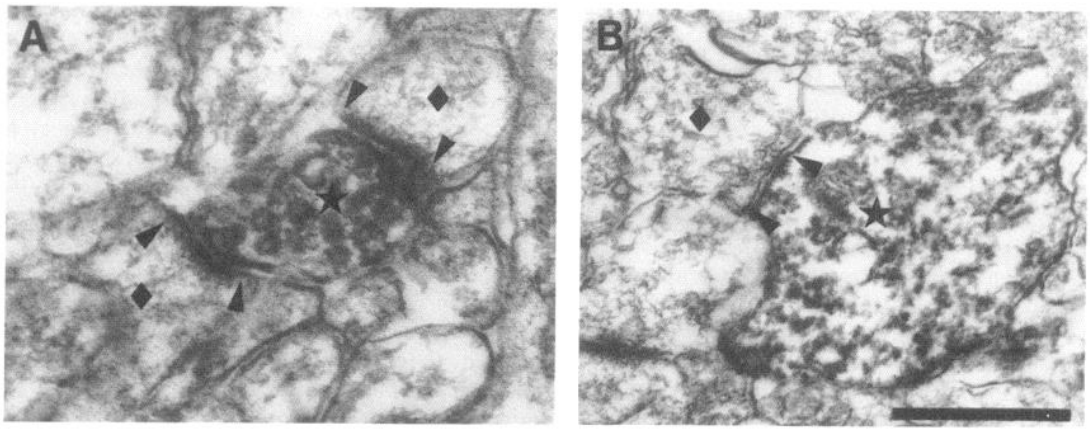

Figure 8. Contrasting localization of mGluR1 and IP_3R viewed at the ultrastructural level. Electron micrographs show the pattern of mGluR1-immunoreactive (*A*) and IP_3R-immunoreactive (*B*) structures. *A* depicts mGluR1-immunoreactive terminal (*star*) forming an asymmetrical synaptic contact (*region between arrowheads*) with two postsynaptic structures (*diamonds*). *B* illustrates a dendrite containing IP_3R immunoreactivity (*star*) receiving a synaptic contact (*region between arrowheads*) from a nonlabeled presynaptic terminal (*diamond*). Scale bar: 0.28 μm for *A*; 0.5 μm for *B*.

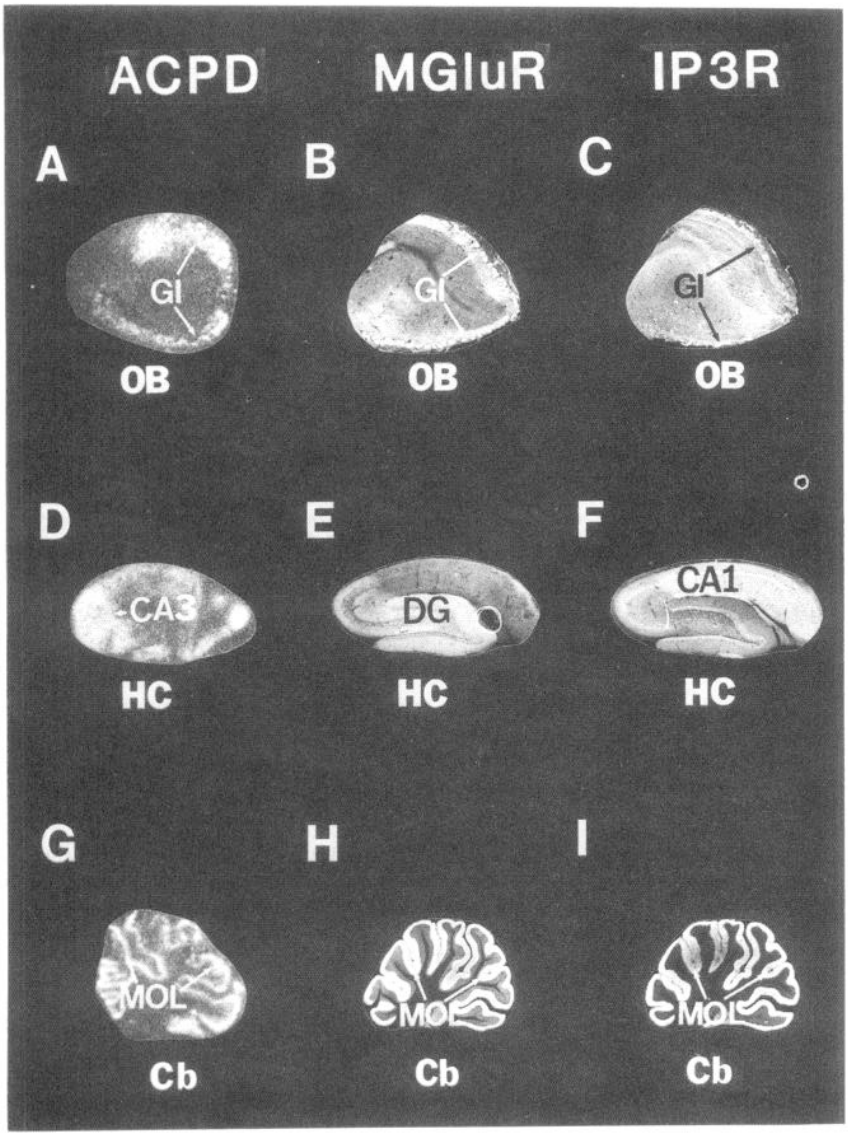

Figure 9. Comparison of the distribution of t-ACPD–stimulated PI imaging with the localization of mGluR1 and IP_3R immunostaining. t-ACPD–stimulated PI turnover (*A, D, G*) occurs in parts of olfactory bulb (*OB*), hippocampus (*HC*), and cerebellum (*Cb*) that contain high amounts of mGluR1 immunostaining (*B, E, H*) whether or not high amounts of IP_3R immunostaining are also present (*C, F, I*). PI imaging in *A, D,* and *G* was carried out as described in the Materials and Methods. In the olfactory bulb (*A–C*) PI imaging is concentrated in the glomeruli (*Gl*), which are also enriched in mGluR1 but not in IP_3R immunoreactivity. Similarly, in the hippocampus (*D–F*), PI imaging is abundant in CA3 and stratum oriens of CA1, regions that contain high and low amounts of mGluR1 and IP_3R, respectively. Interestingly, t-ACPD–stimulated PI turnover is absent from the molecular layer of the dentate gyrus (*DG*), an area with abundant mGluR1 proteins. In the cerebellum (*G–I*), however, PI imaging, mGluR1 and IP_3R proteins are all enriched in the molecular layer (*MOL*).

lipase A_2 (PLA_2) and associated formation of arachidonic acid metabolites can involve G-protein–linked receptors (Piomelli and Greengard, 1990; Marin et al., 1991). Moreover, stimulation by mGluR agonists together with agonists of AMPA receptors enhances the formation of arachidonic acid in cultured striatal neurons (Dumuis et al., 1990). Whether this involves direct activation of PLA_2 or DAG stimulation of PLA_2 (Burch, 1988) awaits further study. The N-type calcium channel labeled by ω-conotoxin (McEnery et al., 1991) is influenced by GTP derivatives and appears linked to G-proteins (Kasai, 1991). mGluR may be associated with a voltage-dependent calcium channel, as quisqualate in the presence of glutamate receptor–gated ion channel antagonists can depress voltage-dependent Ca^{2+} currents in hippocampal neurons in culture in a G-protein–dependent fashion (Lester and Jahr, 1990). The most convincing evidence for the association of other second messengers with mGluR1 comes from Chinese hamster ovary cells expressing this receptor. In these cells, mGluR1 agonists not only enhance PI turnover, but also stimulate the formation of cAMP and the release of arachidonic acid (Aramori and Nakanishi, 1992).

References

Abe T, Sugihara H, Nawa H, Shigemoto R, Mizuno N, Nakanishi S (1992) Molecular characterization of a novel metabotropic glutamate receptor mGluR5 coupled to inositol phosphate/Ca^{2+} signal transduction. J Biol Chem 267:13361–13368.

Aramori I, Nakanishi S (1992) Signal transduction and pharmacological characteristics of a metabotropic glutamate receptor, mGluR1, in transfected CHO cells. Neuron 8:757–765.

Baskys A (1992) Metabotropic receptors and slow excitatory actions of glutamate agonists in the hippocampus. Trends Neurosci 15:92–96.

Baskys A, Malenka RC (1991) Agonists at metabotropic glutamate receptors presynaptically inhibit EPSCs in neonatal rat hippocampus. J Physiol (Lond) 444:687–701.

Berridge MJ, Irvine RF (1989) Inositol phosphates and cell signalling. Nature 341:197–205.

Burch RM (1988) Diacylglycerol stimulates phospholipase A_2 from Swiss 3T3 fibroblasts. FEBS Letts 234:183–286.

Collingridge GL, Lester RAJ (1989) Excitatory amino acid receptors in the vertebrate central nervous system. Pharmacol Rev 40:145–210.

Condorelli DF, Dell Albani P, Casabona AG, Genazzani AA, Sortino MA, Nicoletti F (1992) Development profile of metabotropic glutamate receptor mRNA in rat brain. Mol Pharmacol 41:660–664.

Danoff SK, Ferris CD, Donath C, Fischer G, Munemitsu S, Ullrich A, Snyder SH, Ross CA (1991) Inositol 1,4,5-trisphosphate receptors: distinct neuronal and non-neuronal forms derived by alternative splicing differ in phosphorylation. Proc Natl Acad Sci USA 88:2951–2955.

Dumuis A, Pin JP, Oomagari K, Sebben M, Bockaert J (1990) Arachidonic acid released from striatal neurons by joint stimulation of ionotropic and metabotropic quisqualate receptors. Nature 347:182–184.

Ferris CD, Snyder SH (1992) Inositol 1,4,5-trisphosphate-activated calcium channels. Annu Rev Physiol 54:469–488.

Fotuhi M, Dawson TM, Sharp AH, Martin KJ, Graybiel AM, Snyder SH (1991) The phosphoinositide second messenger system is enriched in striosomes of the primate striatum. Soc Neurosci Abstr 17: 854.

Gerfen CR, Choi WC, Suh PG, Rhee SG (1988) Phospholipase C I and II brain isozymes: immunohistochemical localization in neuronal systems in rat brain. Proc Natl Acad Sci USA 85:3208–3212.

Godfrey PP (1989) Potentiation by lithium of CMP-phosphatidate formation in carbachol-stimulated rat cerebral-cortical slices and its reversal by myo-inositol. Biochem J 258:621–624.

Houamed KM, Kuijper JL, Gilbert TL, Haldeman BA, O'Hara PJ, Mulvihill ER, Almers W, Hagen FS (1991) Cloning, expression, and gene structure of a G protein-coupled glutamate receptor from rat brain. Science 252:1318–1321.

Huang FL, Yoshida Y, Nakabayashi H, Young WS III, Huang K-P (1988) Immunocytochemical localization of protein kinase C isozymes in rat brain. J Neurosci 8:4734–4744.

Hwang PM, Bredt DS, Snyder SH (1990a) Autoradiographic imaging of phosphoinositide turnover in the brain. Science 249:802–804.

Hwang PM, Verma A, Bredt DS, Snyder SH (1990b) Localization of phosphatidylinositol signaling components in rat taste cells: role in bitter taste transduction. Proc Natl Acad Sci USA 87:7395–7399.

Kasai H (1991) Tonic inhibition and rebound facilitation of a neuronal calcium channel by a GTP-binding protein. Proc Natl Acad Sci USA 88:8855–8859.

Kennedy ED, Challiss RAJ, Ragan CI, Nahorski SR (1990) Reduced inositol polyphosphate accumulation and inositol supply induced by lithium in stimulated cerebral cortex slices. Biochem J 267:781–786.

Lester RAJ, Jahr CE (1990) Quisqualate receptor-mediated depression of calcium currents in hippocampal neurons. Neuron 4:741–749.

Lovinger DM (1991) *Trans*-1-aminocyclopentane-1,3-dicarboxylic acid (t-ACPD) decreases synaptic excitation in rat striatal slices through a presynaptic action. Neurosci Lett 129:17–21.

Manzoni OJJ, Finiels-Marlier F, Sassetti I, Blockaert J, le Peuch C, Sladeczek FAJ (1990) The glutamate receptor of the Q_p-type activates protein kinase C and is regulated by protein kinase C. Neurosci Lett 109:146–151.

Marin P, Delumeau JC, Tence M, Cordier J, Glowinski J, Premont J (1991) Somatostatin potentiates the α_1-adrenergic activation of phospholipase C in striatal astrocytes through a mechanism involving arachidonic acid and glutamate. Proc Natl Acad Sci USA 88:9016–9020.

Martin LJ, Blackstone CD, Huganir RL, Price DL (1992) Cellular localization of a metabotropic glutamate receptor in rat brain. Neuron 9:259–270.

Masu M, Tanabe Y, Tsuchida K, Shigemoto R and Nakanishi S (1991) Sequence and expression of a metabotropic glutamate receptor. Nature 349:760–765.

Mayer ML, Westbrook GL (1987) The physiology of excitatory amino acids in the vertebrate central nervous system. Prog Neurobiol 28: 197–276.

McEnery MW, Snowman AM, Sharp AH, Adams ME, Snyder SH (1991) Purified ω-conotoxin GVIA receptor of rat brain resembles a dihydropyridine-sensitive L-type calcium channel. Proc Natl Acad Sci USA 88:11095–11099.

Miller RJ (1991a) Metabotropic excitatory amino acid receptors reveal their true colors. Trends Pharmacol Sci 12:365–367.

Miller RJ (1991b) The revenge of the kainate receptor. Trends Neurosci 11:477–479.

Monaghan DT, Bridges RJ, Cotman CW (1989) The excitatory amino acid receptors: their classes, pharmacology, and distinct properties in the function of the central nervous system. Annu Rev Pharmacol Toxicol 29:365–402.

Nakagawa T, Okano H, Furuichi T, Aruga J, Mikoshiba K (1991a) The subtypes of the mouse inositol 1,4,5-trisphosphate receptor are expressed in tissue-specific and developmentally specific manner. Proc Natl Acad Sci USA 88:6244–6248.

Nakagawa T, Shiota C, Okano H, Mikoshiba K (1991b) Differential localization of alternative spliced transcripts encoding inositol 1,4,5-trisphosphate receptors in mouse cerebellum and hippocampus: *in situ* hybridization study. J Neurochem 57:1807–1810.

Nakanishi S, Maeda N, Mikoshiba K (1991) Immunohistochemical localization of an inositol 1,4,5-triphosphate receptor, P_{400}, in neural tissue: studies in developing and adult mouse brain. J Neurosci 11: 2075–2086.

Nicoletti F, Wroblewski JT, Fadda E, Costa E (1988) Pertussis toxin inhibits signal transduction at a specific metabotropic glutamate receptor in primary cultures of cerebellar granule cells. Neuropharmacology 27:551–556.

Nordquist DT, Kozak CA, Orr HT (1988) cDNA cloning and characterization of three genes uniquely expressed in cerebellum by Purkinje neurons. J Neurosci 8:4780–4789.

Peng Y-W, Sharp AH, Snyder SH, Yau K-W (1991) Localization of the inositol 1,4,5-trisphosphate receptor in synaptic terminals in the vertebrate retina. Neuron 6:525–531.

Piomelli D, Greengard P (1990) Lipoxygenase metabolites of arachidonic acid in neuronal transmembrane signalling. Trends Pharmacol Sci 11:367–373.

Ross CA, MacCumber MW, Glatt CE, Snyder SH (1989) Brain phospholipase C isozymes: differential mRNA localizations by *in situ* hybridization. Proc Natl Acad Sci USA 86:2923–2927.

Ross CA, Danoff SK, Schell MJ, Snyder SH, Ullrich A (1992) Novel inositol 1,4,5-trisphosphate receptors: molecular cloning and differential localization in brain and peripheral tissues. Proc Natl Acad Sci USA 89:4265–4269.

Saito N, Kikkawa U, Nishizuka T, Tanaka C (1988) Distribution of protein kinase C-like immunoreactive neurons in rat brain. J Neurosci 8:369–382.

Schoepp D, Bockaert J, Sladeczek F (1990) Pharmacological and functional characteristics of metabotropic excitatory amino acid receptors. Trends Pharmacol Sci 11:508–515.

Scholz WK, Palfrey HC (1991) Glutamate-stimulated protein phosphorylation in cultured hippocampal pyramidal neurons. J Neurosci 11:2422–2432.

Sharp AH, Dawson TM, Ross CA, Fotuhi M, Mourey RJ, Snyder SH (1992) Inositol 1,4,5-trisphosphate receptors: immunohistochemical localization to discrete areas of rat brain. Neuroscience, in press.

Sladeczek F, Pin J-P, Récasens M, Bockaert J, Weiss S (1985) Glutamate stimulates inositol phosphate formation in striatal neurons. Nature 317:717–719.

Südhof TC, Newton CL, Archer BT III, Mignery GA (1991) Structure of a novel $InsP_3$ receptor. EMBO J 10:3199–3206.

Tanabe Y, Masu M, Ishii T, Shigemoto R, Nakanishi S (1992) A family of metabotropic glutamate receptors. Neuron 8:169–179.

Worley PF, Baraban JM, DeSouza EB, Snyder SH (1986a) Mapping second messenger systems in the brain: differential localizations of adenylate cyclase and protein kinase C. Proc Natl Acad Sci USA 83: 4053–4057.

Worley PF, Baraban JM, Snyder SH (1986b) Heterogeneous localization of protein kinase C in rat brain: autoradiographic analysis of phorbol ester receptor binding. J Neurosci 6:199–207.

Worley PF, Baraban JM, Colvin JS, Snyder SH (1987) Inositol trisphosphate receptor localization in brain: variable stoichiometry with protein kinase C. Nature 325:159–161.

Worley PF, Baraban JM, Snyder SH (1989) Inositol 1,4,5-trisphosphate receptor binding: autoradiographic localization in rat brain. J Neurosci 9:339–346.

Yoshihara C, Saito N, Taniyama K, Tanaka C (1991) Differential localization of four subspecies of protein kinase C in the rat striatum and substantia nigra. J Neurosci 11:690–700.

Young AB, Fagg GE (1990) Excitatory amino acid receptors in the brain: membrane binding and receptor autoradiographic approaches. In: The pharmacology of excitatory amino acids (Lodge D, Collingridge G, eds), pp 18–24. Cambridge: Elsevier.